Published in final edited form as:
Anal Biochem. 2007 May 15; 364(2): 193–203.

Spectroscopic Characterization of Streptavidin Functionalized Quantum dots[1]

Yang Wu‡, **Gabriel P. Lopez**¢, **Larry A. Sklar**‡, and **Tione Buranda**‡

‡*Pathology and Cancer Center, University of New Mexico School of Medicine*

¢*Chemical and Nuclear Engineering, University of New Mexico, Albuquerque, New Mexico, 87131*

Abstract

The spectroscopic properties of quantum dots can be strongly influenced by the conditions of their synthesis. In this work we have characterized several spectroscopic properties of commercial, streptavidin functionalized quantum dots (QD525, lot#1005-0045 and QD585, Lot#0905-0031 from Invitrogen). This is the first step in the development of calibration beads, to be used in a generalizable quantification scheme of multiple fluorescent tags in flow cytometry or microscopy applications. We used light absorption, photoexcitation, and emission spectra, together with excited-state lifetime measurements to characterize their spectroscopic behavior, concentrating on the 400-500nm wavelength ranges that are important in biological applications. Our data show an anomalous dependence of emission spectrum, lifetimes, and quantum yield (QY) on excitation wavelength that is particularly pronounced in the QD525. For QD525, QY values ranged from 0.2 at 480nm excitation up to 0.4 at 450nm and down again to 0.15 at 350nm. For QD585, QY values were constant at 0.2 between 500nm and 400nm, but dropped to 0.1 at 350nm. We attribute the wavelength dependences to heterogeneity in size and surface defects in the QD525, consistent with characteristics previously described in the chemistry literature. The results are discussed in the context of bridging the gap between what is currently known in the physical chemistry literature of quantum dots, and the quantitative needs of assay development in biological applications.

Keywords

nanotechnology; quantum dots; excited state spectroscopy; quantum yield; calibration beads; flow cytometry; fluorescence lifetime; biosassays

Introduction

Over the past few years, there has been increasing interest in the use of quantum dots as fluorescent tags in biology(1-7). Quantum dots are semiconductor nanoparticles with tunable optical properties that are strongly dependent on size (8). In a large sample of semiconductor material, the lowest electronically excited state features an electron and a hole orbiting each other (a Wannier exciton(9)). The distance that separates the electron and the hole is called the

[1]This work was supported by NIHK25AI 60036 (TB), NSF CTS0332315 (GPL) and U54MH074425 (LAS). TB thanks Drs Ralph Young (Eastman Kodak, Rochester, NY) and John Endicott (Wayne State, Detroit, MI) for stimulating discussions on excited state spectroscopy and critical comments through out the progress of this work. Flow Cytometry was also supported by NCIP30CA118100.

corresponding author: Tione Buranda University of New Mexico School of Medicine Department of Pathology 224 CRF Building 229 MSC084630 Albuquerque, NM 87131 e-mail: Buranda@unm.edu phone: 505-272-1259 FAX: 505-272-6995

Bohr radius of the exciton, and its magnitude depends on the composition of the semiconductor material (typically 20-80Å for group II-VI semiconductors(10); 56Å for CdSe (11)). If the size of a nanocrystal is less than the Bohr radius for the material, the electronic wavefunctions and energies are altered by the boundaries (quantum confinement)(11,12). Whereas a large sample has a quasicontinuum of electronic excited states, those of a quantum dot are split into discrete states and shifted to higher energies. Thus, the absorption and emission associated with the lowest-energy electronic transition are narrowed, and they shift to higher energies as the size of the quantum dot decreases. The discrete nature of the electronic transitions of individual dots is typically obscured by sample inhomogeneities such as distribution in size, shape and stoichiometry (13,14).

To make them suitable for biological applications, quantum dots must be passivated (2,15). Passivation is a chemical process by which a dot (the core) is surrounded by another material of a larger optical bandgap (the shell). CdSe dots are commonly passivated with a ZnS shell to prevent the contamination of the core material, and improve the optical properties of the nanocrystal (1,2). The surface is then covalently attached to a layer of organic ligand, which interacts with the hydrophobic part of a polymer layer. The outer part of the polymer coating is hydrophilic and functionalized with carboxylic acid derivatives, and can thus be functionalized with molecules of biological interest (2).

Biofunctionalized quantum dots are presently available from commercial sources. The spectroscopic properties of dots are dependent on their size distribution, shape, and surface defects (13,14,16-25). Subtle differences in preparation can lead to batch-to-batch variation in basic spectroscopic properties such as luminescence quantum yield (13,14,16-25). To the best of our knowledge, the commercial dots are not spectroscopically standardized, nor are they characterized completely enough in the product literature for them to be used without further evaluation(16).

In this work we have characterized several spectroscopic properties of commercial (Invitrogen) streptavidin-functionalized quantum dots as a first step in the development of fluorescent calibration beads for flow cytometry. We have focused on two samples of CdSe quantum dots, with emission bands centered at 525 nm (QD525 lot#1005-0045) and 585 nm (QD585 Lot#0905-0031). We cite the lot numbers here to emphasize the notion that, unlike molecular dyes, the spectroscopic characteristics of quantum dots can be influenced by details of their synthetic history (16). Thus the quantitative data presented here are most appropriate for the samples from the indicated lots. Nevertheless, they illustrate the concerns that arise when one attempts to use a previously uncharacterized batch of dots. These specific quantum dots were chosen because they can be readily analyzed through the optics of standard Becton Dickinson (BD) flow cytometers, which are available in numerous labs. We used light absorption, photoexcitation, and emission spectra, together with excited-state lifetime measurements to characterize their spectroscopic behavior, concentrating on wavelength ranges that are important in biological applications. Our data show an anomalous dependence of emission spectrum and yield on excitation wavelength that are particularly pronounced in the QD525. We attribute this behavior to size heterogeneity and surface defects in the QD525, consistent with tendencies previously described in the literature (16,24,25). The results are discussed in the context of bridging the gap between what is currently known in the physical chemistry literature of quantum dots, and the quantitative needs of assay development in biological applications (26).

MATERIALS AND METHODS

Materials

Streptavidin coated and biotin coated polystyrene particles (6.7 μm in diameter, 0.5% w/v) were purchased from Spherotech Inc. (Libertyville, IL). Streptavidin coated quantum dots QD525 and QD585 were purchased from Invitrogen Corp. (Carlsbad, CA). QD605 was obtained from the erstwhile Quantum Dot Corp. FLAG peptide (DYKDDDDK), M2 anti-FLAG antibody and paraformaldehyde (PFA), were purchased from from Sigma (St. Louis, MO). Phosphate-buffered saline (PBS) was purchased from Mediatech, Inc, Herndon, VA). Biotinylated FLAG ($FLAG^{bio}$) and FITC conjugated FLAG peptides ($FLAG^{FITC}$) were synthesized at UNM as described elsewhere(27). TRIS (10 mM or 25 mM Tris, 150 mM NaCl, pH 7.5) and HHB (30 mM HEPES, 110 mM NaCl, 10 mM KCl, 1mM $MgCl_26H_2O$ and 10 mM glucose, pH 7.4) buffer were used in the presence or absence of 0.1% bovine serum albumin (BSA).

Determination of the relative emission yields of quantum dots

Absorption and spectrofluorometric measurements were performed using a Hitachi model U-3270 spectrophotometer (San Jose, CA) and a Photon Technology International QuantaMaster™ Model QM-4/2005 spectrofluorometer (Lawrenceville, NJ) respectively. QD525, QD585, QD605, fluorescein, FITC biotin, FITC labeled FLAG peptide ($FLAG^{FITC}$) and Rhodamine B solutions were prepared in PBS (pH 7.4 or pH 8.0). The optical densities of all the samples were matched at either 405 nm or 488 nm. Excitation spectra were collected for all samples using a 16 nm bandpass at the excitation and detection monochromators. Emission spectra were measured with 2nm bandpass at the excitation and emission monochromators.

Correcting excitation spectra for spectral distribution of the lamp

An uncorrected excitation spectrum differs from the “true” spectrum primarily because of the spectral distribution (L_λ) of the lamp (28) where the latter varies according to the characteristics of the lamp and monochromators. In cases where a spetrofluorometer instrument lacks the capability to automatically perform a correction of L_λ of excitation spectra, several manual approaches which involve the evaluation of L_λ have been described elsewhere (28,29). For a dilute solution, the true excitation spectrum is directly proportional to the quantity $\varepsilon\varphi_f$ (where ε is the extinction coefficient and φ_f is the quantum yield). Since for many organic fluorophores, φ_f is independent of the wavelength of the exciting light, the true excitation spectrum is a replica of the absorption spectrum *i.e*. Kasha's rule (30). Because of Kasha rule, the lineshape of L_λ can be extracted from a comparison of the raw excitation spectrum of common standard dyes like fluorescein and rhodamine with their corresponding absorption spectra (29). The imprint of L_λ in an excitation spectrum can be extracted by dividing a normalized excitation spectrum with the normalized absorption spectrum of the standard solution. The resulting plot of L_λ can then be used to correct the excitation spectra of the non standard samples (Qdots) (28,29).

Reduced Emission Spectra

Emission spectra were acquired as photons per unit wavelength (λ) and initially plotted versus wavelength (I_λ). Analysis of the data is usually more straightforward for spectra expressed in photons per unit energy, frequency or wavenumber ($\nu = 1/\lambda$), namely I_ν (29). The two representations are related by $I_\nu\,|d\nu| = I_\lambda\,|d\lambda|$, or $I_\nu = I_\lambda/\nu^2$. To analyze spectral profiles, it is convenient to remove an additional factor of ν^3 that arises from coupling of the transition moment(s) to the radiation field(31). Therefore, for purposes of analysis, emission spectra were plotted as *reduced spectra* (32), i.e., I_λ/ν^5 versus ν.

Fluorescence Lifetime Measurements

Fluorescence lifetime measurements of dots, fluorescein and fluorescein conjugates, were performed on a Model TM-3/2005 Lifetime Spectrofluorometer from Photon Technologies International (PTI). The out put (pulsewidth; ≈ 800 ps, repetition rate; 10 Hz) from a GL-3300 Nitrogen pumped Dye laser (Model GL-302) was used to excite the probes at various wavelengths between 420 nm and 500 nm. Data collection and analysis was performed using the FeliX32™ Advanced Fluorescence Analysis Software Package (PTI). In a typical experiment, a 40 μL cuvette was placed in the spectrofluorometer's temperature-controlled sample holder. Lifetime measurements were performed at room temperature.

RESULTS

Some Basic Spectroscopic Properties of Quantum dots: (a) Absorption Spectra

Figure 1A shows the absorption spectra of fluorescein and dots, where the optical densities of the fluorophores were all matched at 488 nm. The absorption spectrum of fluorescein (*a* in Figure 1A) has textbook features, and fluorescein is used here as a fluorescence standard with known spectroscopic characteristics (29). The lowest energy band in the absorption spectra of the quantum dots is labeled $1S_{3/2}$<—$1S_e$, where $1S_{3/2}$ and $1S_e$ are conventional descriptors for the HOMO and LUMO of a CdSe dot and the arrow points in the direction of the electronic transition (33). Higher energy transitions (e.g., $1P_{3/2} \leftarrow 1S_e$) appear as shoulders on a continuum of increasing extinction coefficient with decreasing wavelengths (10). Spectral hole burning experiments have shown the fine structure of the electronic transitions buried under the broad bands which correspond to atomic transitions of single dots (10). The energy level of the band edge transition is a characteristic of the size of the dot (34). A useful theoretical formula has been developed to correlate the absorbance maximum of the lowest-energy transition to the size of the core of the quantum dot. This is shown in its simplified algebraic form in Equation 1(8).

$$E_{1S_{3/2}<-1S_e} = E_g + R_y^*\left[\pi^2\left(\frac{a_b}{a_{dot}}\right)^2 - 1.786\left(\frac{a_b}{a_{dot}}\right) - 0.248\right] \quad (1)$$

Here, $E_{1S_{3/2}<-1S_e}$ is the energy of the first electronic transition, as calculated from the absorption spectrum (2.4 eV for QD525; 2.16 eV for QD585), E_g is the band-gap energy for bulk material (1.84 eV for CdSe), a_b is the exciton Bohr radius (5.6 nm for CdSe), a_{dot}= radius of the Qdot, and R_y* is the Rydberg constant (0.016 eV for CdSe) (8,10,11). We can thus estimate the respective core sizes of QD525 (b in Figure 1A) and QD585 (c in Figure 1A) to be 2.8 nm and 3.6 nm. Very nearly the same values are obtained using the experimental size calibration curves published by Peng *et al* (35). It is worth noting that after passivation (15) and biological functionalization (2) the net size of the dot is on the order of 10-15nm according to the product literature (www.probes.invitrogen.com).

Excitation and Emission spectra

To analyze the photo excitation spectra, we began by correcting for the uneven spectral distribution (L_λ) of the lamp (28) as described in the methods. The corrected spectra are shown in Figure 1B. According to Kasha's rule, the emission spectrum and quantum yield should be independent of the excitation wavelength (37). For the present, dilute samples the photoexcitation spectrum should be proportional to the absorbance spectrum. Unlike the case of fluorescein, photoexcitation spectra of the dots do not match the absorption spectrum (e.g. Figure 2A). One potential cause for this anomalous behavior is sample heterogeneity. The emission spectra of the dots are sensitive to their size, with smaller dots emitting bluer light than larger dots (21-23,36). The photo excitation spectrum of QD525 (shown in figure 1B) was collected at 525 nm using a fairly broad bandpass for excitation and detection (16 nm). Even

so, in a heterogeneous sample, the data thus collected are likely to be biased in favor of those dots whose emission maxima are near the detection wavelength. In principle one can probe the size distribution of the dots by selecting detection wavelengths on either the blue or the red side of the emission spectra (data not shown). Alternatively, one can examine the emission spectra obtained with various excitation wavelengths. We collected a series of emission spectra, exciting at the wavelengths marked with asterisks in Figure 2A. To optimize the ability to resolve different sized dots, we set the slitwidths to a 2nm bandpass for both excitation and emission. The results are summarized in Figure 2B and Table 1.

In Table 1 we have listed the emission maxima and spectral bandwidths (FWHM) measured for each excitation wavelength. The emission spectra between 465 and 515 nm were found to be sensitive to excitation wavelength and varied in terms of their respective band maxima and widths. For example, excitation of the sample at 470 nm (abbreviated 470EX hereafter) produced an emission spectrum that was red shifted by 6nm relative to the 525nm maxima of the "parent" system indicating the photoselection of relatively larger dots(8,20,24,25,36). In contrast, excitation at 490 nm (490EX) yielded an emission spectrum with a 7nm blue shift signifying the photoselection of smaller dots at this excitation wavelength(20,36). Excitation at 480 nm produced a very broad (44nm FWHM, compared to ~30 nm for the other spectra) low intensity band centered at 525 nm. At excitation wavelengths between 490 and 515 nm the emission maximum gradually returned to the nominal value of 525 nm (*cf.* 515EX excitation in Figure 2B).

In contrast, the band maxima and FWHM of QD585 did not change significantly from 585 nm and 28 nm, respectively throughout the excitation window from 400 nm to 575 nm (Table 1).

Kasha's rule (30) – that the emission spectrum should be independent of the excitation wavelength – applies if (a) excitation at any wavelength leads to the same excited state with the same probability (here, the lowest excited state of a dot and unit probability), and (b) only one species is present (here, dots of identical size and shape). The differences in the shapes of the excitation and absorption spectra at shorter wavelengths ($\leq$ 420 nm) are believed to represent a violation of the first condition (37,38). Such a violation would affect the overall intensities, but not the shapes of the emission spectra. The deviations at longer excitation wavelengths, of greater interest for our practical application, appear to represent a violation of the second condition, i.e. a heterogeneous sample of dots. Evidence for sample heterogeneity is summarized in Figure 3 where the QD525 dots were probed between 470nm and 490nm.

To illustrate that the varying spectra can be understood in terms of a distribution of dot sizes (or shapes), we have plotted the spectra (reduced and normalized) resulting from excitation at 470nm, 480nm, and 490nm (a, c, and b respectively in Figure 3A). The variations over this narrow range of excitation wavelength are particularly striking. The 480EX spectrum can be reproduced, approximately, by averaging the 470EX and 490EX spectra. This is the expected result if 470EX (or 490EX) excites a population of larger (or smaller dots), and 480EX excites the two populations equally. The extra breadth of the 480EX spectrum is a consequence of this less selective excitation. Taken at face value, the 470EX and 490EX spectra represent dots of core radii 2.9 and 2.5 nm, respectively- as calculated from Equation 1. The 480EX spectrum is reproduced fairly well, but not perfectly. Taking a weighted average and optimizing the weights does not change the situation. There are clearly more than two distinct populations of sizes and/or shapes.

Within the 470nm –490nm range of excitation wavelengths, it seems counterintuitive that redder excitation (490 nm) yielded a blue shifted spectrum and bluer excitation (470 nm), 470EX produced a red shifted spectrum relative to the putative "parent" band maxima of 525nm. To rationalize this result, we turn to Figure 3B. The two curves are an instructive model

representation of the overlapping absorption spectra of small dots and large dots. The peak of the lowest electronic transition ($1S_{3/2}$<—$1S_e$) of the larger dots is shown at nominally lower energy than the smaller dots as one might expect (8). The spectral mismatch (≈20nm) of the two model dots is such that the peak of the $1S_{3/2}$<—$1S_e$ transition associated with the smaller dots is centered at 490nm. Consequently, the onset of the next highest $1P_{3/2}$<—$1S_e$ transition occurs in the 470nm region of the spectrum where it overlaps with the trough in the absorption spectrum of the smaller dots. The excitation wavelengths of interest are marked by asterisks in Figure 3B. In this model, at 470 nm (or 490 nm), the larger (or smaller) dots absorb more strongly and are excited somewhat selectively, and the emission maximum tends to that of the larger (or smaller) dots. (At 480 nm, the two populations are excited equally.)

Quantum Yields

Emission yields of dots were determined from the analysis of the integrated emission intensities of the dots relative to fluorescein or rhodamine B (QD585). QD525 and fluorescein were absorbance-matched and excited at 420 nm and 490, while QD585 and Rhodamine B were absorbance-matched and excited at 488 nm. The quantum yields were derived as described in Note *3* of Table 2. Figure 4 shows the emission bands of fluorescein, rhodamine B, QD525 and QD585, the intensities are shown normalized to optical densities at the excitation wavelengths. Thus, their magnitudes as shown, are nearly proportional to their quantum yields relative to fluorescein (*cf.* Note 3 in Table 2).

To estimate the quantum yield per unit wavelength, between 400 and 500 nm, for fluorescein and each dot sample, we divided the excitation spectra (Figure 1B) with the absorption spectrum (Figure 1A). The quantum yield values were then scaled to the emission yields measured at 420EX (0.37 for QD525) and 488EX (0.20 for QD585). The results are shown in Figure 5. In Figure 5 we have included the quantum yield determination of a 4 year old sample of QD605 (from the erstwhile *Quantum Dot Corp*.) for reference purposes. As noted the spectroscopic behavior of these dots was very close to those of QD585. QD585 and QD605 were largely constant between 425 and 500 nm. For the QD525 sample, the emission yield changed from a high of 0.4 at 450nmEX to the low of 0.20 at 480EX. This behavior was attributed to sample heterogeneity as discussed below. It is important to recognize that quantum yields that are derived from excitation spectra are more likely to be biased towards reporting the emission yield of dots whose emission band maxima are centered at the wavelength of detection when probing a heterogeneous sample *(vide supra).* Evidence for this bias is shown in the QD525 data (*b* in Figure 5) where the wavelength-specific quantum yield values that were derived from excitation spectra markedly deviate (475-500nm measurement window) from the results that were derived from data based on integrated emission.

Excited State Lifetimes

We used excited state lifetime measurements to elucidate the differences in the excited state behavior of small and large dots in the QD525 and QD585 samples. In principle we expected to selectively probe the excited state lifetimes of smaller and larger dots by profiling the blue edges and the red edges of the emission spectra respectively (17,39,40). Figure 6A shows an overlay of emission spectra measured at the following excitation wavelengths: (a) 438EX, (b) 470EX, (c) 480EX and (d) 490EX. The arrows indicate the detection wavelengths at which the luminescence decay lifetimes were analyzed. Emission intensity decay data were collected at room temperature and were analyzed using PTI's FELIX™ software. The data are summarized in Figure 6B and 6C. Figure 6B shows a semilog 3D plot of emission intensity decays of excited state species profiled along the 438EX band (***a*** in Figure 6A). At 438Ex the emission lifetimes of the species emitting blue edge photons (i.e. 500 nm and 510 nm) were nominally biphasic, yielding 15.0±1.0ns and 22.0±1 ns lifetimes of comparable amplitudes. The excited state decay of the species emitting red edge photons (530-540 nm) was single-exponential; 22±0.1ns.

These fluorescence decay characteristics were typical of excitations at wavelengths <465 nm. Our analysis of QD585 samples found lifetimes to be largely single exponential ≈ 22ns over the wavelength range from 420EX to 570EX. Because the QD585 dots appeared well behaved, we did not profile the emission spectra of these dots in the same detail as the QD525 dots.

Figure 6C shows a 3D plot of emission decays from the profile of 480EX (***c*** in 6A). The data shown are representative of the decay profiles of excitation within the 470-590 nm spectral region where probing the blue edges (500-510nm) of the emission spectra ***b***-***d*** in Figure 6A were dominated by intense Rayleigh scattering (41) of light identifiable by its temporal characteristics which matched our laser (800ps pulsewidth). The scatter was on the order of 100 times the emission signal. Because of this extremely high background we did not attempt to extract lifetimes from these data.

Figure 7 shows typical excited stated decay characteristics of QD525 dots. In general, excitation at wavelengths below 460 nm and then at wavelengths longer than 500nm obtained excited state species with single exponential decays. On the other hand, in exciting the sample at wavelengths between 465 and 490 nm, multiexponential decays were observed. In this spectral region, laser excitation was in resonance with overlapping electronic transitions that corresponded to dots of different sizes. We therefore obtained multiphasic decays as shown in Figure 7B. To summarize the general *qualitative* trends, the blue edge photons (500-510) from 480EX and 490EX experiments qualitatively appeared to be associated with excited state species of relatively short lifetimes <10ns (much shorter than the excited state species emitting blue edge photons that were the progeny of excitations at wavelengths <460nm. The excited state species emitting red edge photons in the emission spectra in this region exhibited excited state lifetimes ranging from <10, 15.4 ns to 23ns.

Discussion

In this study we have examined some spectroscopic properties of commercial streptavidin functionalized dots with the view of advancing a rational basis for developing calibration beads (42,43) based on quantum dots (26). In this work we have relied on the theoretical and experimental framework established by the earlier work of Brus *et al* (10,11,44,45), Bawendi *et al* (18,19,22,23,46-49) and others (15,24,25,50,51). Experimental data have shown a strong correlation between the method of dot preparation and excited state behavior (23). Several authors reported a decrease of emission yield with decreasing wavelength, suggesting an anomalous dependence of excitation on wavelength (24,25,37,38,52). Potential mechanisms for this process have been postulated, including the hypothesized existence of electronic relaxation channels of “hot” electrons, which bypass the lowest excited state (37,38). More recent studies have suggested that the deviation between the absorption and photoexcitation spectra may be in part accounted for by artifacts of size dispersion, light scatter and preparation history of the dots (16). The preparative history of commercial dots is largely unknown to the end user. Therefore in this study, we have used three different experimental measures of the spectroscopic properties of a pair of different sized dots, in order to evaluate their ground state properties relative to the excited state.

On the Correspondence of Absorption and Photoexcitation Spectra of QD525 and QD585 Qdots

To accurately evaluate the emission yield as a function of excitation wavelength it is necessary to perform measurements at optical densities below 0.1. In this limit, errors due to inner filter effects alone are on the order of 10% (28). Experiments performed at or above this threshold, or in cases were light scatter is a concern, require a correction for the actual number of photons absorbed rather than relying on the measured absorbance (16,24,25). The fraction of photons absorbed is proportional to *1-T*; where $T=I/I_0$ is the fraction of transmitted light, with I_0 being

the incident light and *I* the transmitted light. It has been shown that 1-T is within 10% of measured absorbance when the optical density is < 0.1(16). In our experiments the optical densities were limited to ≤ 0.02 at 400 nm where the subsequent error in φ□ due to inner filter effects is 2% (28).

Photoexcitation spectra are shown in Figure 1B. Based on the quantum yield calculation (Figure 5), the excitation spectrum of the QD585 dots appears to essentially replicate the absorption spectrum between the 400 nm and 500 nm interval. However, the quantum yield appears to fall by 50% at 350nm. In contrast, the quantum yield of the QD525 dots is seriously dependent on excitation wavelength in the same wavelength window (400-500 nm) where the QD585 dots appear to be consistent with expectation. The emission yield of the QD525 dots also significantly drops to 15% at 350 nm from a high of 40% at 450 nm. The level of drop (≤50%) in quantum yield at the high-energy end for both samples is consistent with literature reports (16,52). The difference in behavior between the QD525 and QD585 dots appears to originate more from differences in size distribution rather than intrinsic properties where the smaller QD525 dots appear to be more heterogeneous (*c.f.* Table 1 and Figure 2).

Emission Spectra and Radiative lifetimes

Emission spectra and lifetime measurements provide a complementary experimental measure for delineating the influence of size distribution and purity of dot populations (40,53). The differences in the emission spectra in terms of bandwidth and band maxima of the QD525 dots (Figure 2) are very striking relative to the QD585 samples (Table 1).

In our fluorescence lifetime measurements, we profiled the emission spectra by measuring the excited state lifetimes of the species emitting photons localized in the blue (smaller dots) and red (larger dots) edges of the spectrum(17,39,40). Our analysis of the excited state decays along the blue edges of the emission spectra between 470EX and 490EX were hindered by strong resonance Rayleigh scatter (29). It turns out that resonant Raleigh scattering can be strongly enhanced in the vicinity of areas of inhomogenous broadening of electronic transitions, arising from a finite distribution of sizes (*cf.* Table 1) (41). It is worth noting that Rayleigh scatter of this magnitude was neither observed when QD585 samples at wavelengths correspondingly near to the detection wavelength for this sample, nor at shorter wavelengths e.g. 420EX, or 438EX even though one would expect more scatter in the blue region due to the ν^{-4} dependence of scattering phenomenon (29).

In summary our spectroscopic characterization of the QD525 and QD585 dots shows that the larger QD585 dots are fairly “monodisperse” and have a fairly constant quantum yield when excited between the commonly used excitation window of 400 and 500 nm. Several factors including size heterogeneity and potential impurities (*c.f.* resonance Rayleigh scatter) appear to cause the anomalous variations in the quantum yield of the QD525 dots when excited between 400 and 500 nm. While the wavelength dependent quantum yield of the 525 dots is twice as high (40%), at some wavelengths, as the QD585 (20%), unfortunately it drops to 20% in the 490 nm region, which represents an important excitation window in flow cytometry and microscopy.

Some Practical considerations of Qdots in flow cytometry and microscopy

We will now attempt to present a measurement model that provides a framework intended to translate the results of the present spectroscopic characterization to the development of calibration beads as described elsewhere (26). In flow cytometry, the quantitation of fluorophore tagged ligands and receptors, is achieved by the use of standard beads of known calibration (42,43). The calibration beads that are currently available are targeted towards a handful of specific fluorophores (e.g. fluorescein). In order to develop a general use calibration

bead, it is useful to derive a simple ratiometric formula for comparing the number of fluorophores of *Sample 1*: an analyte, capable of emitting radiation of intensity I_1 that is equivalent to a single unit of *Sample 2*: a calibration standard. For simplicity both samples must be excited at the same wavelength, using *non-saturating* light intensity, and emit in the same spectral region as defined by the same bandpass filter. Equation 2 shows a formalism derived from simple spectroscopic parameters; extinction coefficients (ε), quantum yields (φ), and the bandpass transmittance (%T) of sample emission. Equation 1 allows one to determine the number density (ρ_i) of sample analyte molecules with calibration beads.

$$\frac{I_1}{I_2} = \frac{\epsilon_{\lambda,1}}{\epsilon_{\lambda,2}} \cdot \frac{\varphi_1}{\varphi_2} \cdot \frac{\%T_1}{\%T_2} \cdot \frac{\rho_1}{\rho_2} \quad (2)$$

In Equation 1, ε can be readily measured from absorption spectra for most probes. The quantum yields φ_i can be determined by the end-user relative to known textbook standards (28,29). Because dots are not yet fully standardized one would like to verify basic spectroscopic properties beginning with photoexcitation spectra as described here. In Figure 4 we have overlaid the emission spectra of fluorescein, QD525, and QD585 with bandpass filter cross sections associated with the two detection channels (FL1 and FL2) of a model BD flow cytometer. The filters are a 30 nm band pass filter centered at 530 nm (515 nm ≤ 530 ≤ 545 nm) and a 42 nm bandpass filter centered at 585nm (564 nm ≤ 585 ≤ 606 nm). Only 28% fluorescein's emission radiance is transmitted to the detector. For the dots, the emission bands are relatively narrow and symmetrical, thus a larger percentage of radiance is transmitted. Interestingly, based on our current study, the heterogeneity in the QD525 sample results in a differential spectral mismatch with the bandpass filter such that 48% or 38% of total intensity is transmitted if the sample is excited at 450 nm or 488 nm respectively. As it turns out, the most common excitation line used in an Argon ion laser is 488 nm, where the selective photo excitation of the smaller sized dots with a blue shifted, 518 nm, emission band is recorded. On the other hand, over 90% of QD585 is transmitted. Having described all the necessary spectroscopic parameters herein, (Table 2) elsewhere (26) we have described the assembly of quantum dots with known surface density (ρ_2 in Equation 1) on beads, in order to test and demonstrate the applicability of these beads as calibrations standards.

References

1. Michalet X, Kapanidis AN, Laurence T, Pinaud F, Doose S, Pflughoefft M, Weiss S. The power and prospects of fluorescence microscopies and spectroscopies. Annual Review Of Biophysics And Biomolecular Structure 2003;32:161–182.
2. Michalet X, Pinaud FF, Bentolila LA, Tsay JM, Doose S, Li JJ, Sundaresan G, Wu AM, Gambhir SS, Weiss S. Quantum dots for live cells, in vivo imaging, and diagnostics. Science 2005;28:538–544. [PubMed: 15681376]
3. Pinaud F, King D, Moore HP, Weiss S. Bioactivation and cell targeting of semiconductor CdSe/ZnS nanocrystals with phytochelatin-related peptides. Journal Of The American Chemical Society 2004;19:6115–6123. [PubMed: 15137777]
4. Michalet X, Pinaud F, Lacoste TD, Dahan M, Bruchez MP, Alivisatos AP, Weiss S. Properties of fluorescent semiconductor nanocrystals and their application to biological labeling. Single Molecules 2001;2:261–276.
5. Alivisatos P. The use of nanocrystals in biological detection. Nature Biotechnology 2004;22:47–52.
6. Bruchez M, Moronne M, Gin P, Weiss S, Alivisatos AP. Semiconductor nanocrystals as fluorescent biological labels. Science 1998;25:2013–2016. [PubMed: 9748157]
7. Lidke DS, Nagy P, Heintzmann R, Arndt-Jovin DJ, Post JN, Grecco HE, Jares-Erijman EA, Jovin TM. Quantum dot ligands provide new insights into erbB/HER receptor-mediated signal transduction. Nature Biotechnology 2004;22:198–203.

8. Gaponenko, SV. Optical Properties of Semiconductor Nanocrystals. Cambridge University Press; Cambridge: 1998.
9. Hopfield JJ. Theory of the Contribution of Excitons to the Complex Dielectric Constant of Crystals. Physical Review 1958;112:1555–1567.
10. Alivisatos AP, Harris AL, Levinos NJ, Steigerwald ML, Brus LE. Electronic States of Semiconductor Clusters - Homogeneous and Inhomogeneous Broadening of the Optical-Spectrum. Journal Of Chemical Physics 1988;1:4001–4011.
11. Nirmal M, Brus L. Luminescence Photophysics in Semiconductor Nanocrystals. Acc. Chem. Res 1999;32:407–414.
12. Wang LW, Zunger A. High-energy excitonic transitions in CdSe quantum dots. Journal Of Physical Chemistry B 1998;20:6449–6454.
13. Dabbousi BO, RodriguezViejo J, Mikulec FV, Heine JR, Mattoussi H, Ober R, Jensen KF, Bawendi MG. (CdSe)ZnS core-shell quantum dots: Synthesis and characterization of a size series of highly luminescent nanocrystallites. Journal Of Physical Chemistry B 1997;13:9463–9475.
14. Danek M, Jensen KF, Murray CB, Bawendi MG. Synthesis of luminescent thin-film CdSe/ZnSe quantum dot composites using CdSe quantum dots passivated with an overlayer of ZnSe. Chemistry Of Materials 1996;8:173–180.
15. Alivisatos AP. Semiconductor clusters, nanocrystals, and quantum dots. Science 1996;16:933–937.
16. Tonti D, van Mourik F, Chergui M. On the excitation wavelength dependence of the luminescence yield of colloidal CdSe quantum dots. Nano Letters 2004;4:2483–2487.
17. Caruge JM, Chan YT, Sundar V, Eisler HJ, Bawendi MG. Transient photoluminescence and simultaneous amplified spontaneous emission from multiexciton states in CdSe quantum dots. Physical Review B 2004;70:085316.
18. Efros AL, Rosen M, Kuno M, Nirmal M, Norris DJ, Bawendi M. Band-edge exciton in quantum dots of semiconductors with a degenerate valence band: Dark and bright exciton states. Physical Review B 1996;15:4843–4856.
19. Kuno M, Lee JK, Dabbousi BO, Mikulec FV, Bawendi MG. The band edge luminescence of surface modified CdSe nanocrystallites: Probing the luminescing state. Journal Of Chemical Physics 1997;15:9869–9882.
20. Norris DJ, Nirmal M, Murray CB, Sacra A, Bawendi MG. Size-Dependent Optical Spectroscopy of Ii-Vi Semiconductor Nanocrystallites (Quantum Dots). Zeitschrift Fur Physik D Atoms Molecules And Clusters 1993;26:1–4.
21. Norris DJ, Sacra A, Murray CB, Bawendi MG. Measurement of the Size-Dependent Hole Spectrum in Cdse Quantum Dots. Physical Review Letters 1994;18:2612–2615. [PubMed: 10055928]
22. Norris DJ, Bawendi MG. Structure in the Lowest Absorption Feature of Cdse Quantum Dots. Journal Of Chemical Physics 1995;1:5260–5268.
23. Norris DJ, Bawendi MG. Measurement and assignment of the size-dependent optical spectrum in CdSe quantum dots. Physical Review B 1996;15:16338–16346.
24. Rumbles G, Selmarten DC, Ellingson RJ, Blackburn JL, Yu PR, Smith BB, Micic OI, Nozik AJ. Anomalies in the linear absorption, transient absorption, photoluminescence and photoluminescence excitation spectroscopies of colloidal InP quantum dots. Journal Of Photochemistry And Photobiology A Chemistry 2001;14:2–3.
25. Ellingson RJ, Blackburn JL, Yu PR, Rumbles G, Micic OI, Nozik AJ. Excitation energy dependent efficiency of charge carrier relaxation and photoluminescence in colloidal InP quantum dots. Journal Of Physical Chemistry B 2002;15:7758–7765.
26. Wu Y, Campos S, Lopez G, Ozbun MA, Sklar L, Buranda T. The Development of Quantum Dot Calibration Beads and Quantitative Multicolor Bioassays in Flow Cytometry. Anal. Biochem. 2006submitted
27. Buranda T, Lopez GP, Simons P, Pastuszyn A, Sklar LA. Detection of epitope-tagged proteins in flow cytometry: Fluorescence resonance energy transfer-based assays on beads with femtomole resolution. Analytical Biochemistry 2001;298:151–162. [PubMed: 11700971]
28. Parker, CA. Photoluminescence of solutions. Elsevier; Amsterdam: 1968.
29. Lakowicz, JR. Principles of Fluorescence Spectroscopy. Plenum Press; New York: 1999.

30. Kasha M. Characterization of Electronic Transitions in Complex Molecules. Discussions of the Faraday Society 1950;9:14–19.
31. Mulliken, RS.; Person, WB. Molecular complexes: a lecture and reprint volume. Wiley; New York: 1969.
32. Gould IR, Noukakis D, Gomezjahn L, Young RH, Goodman JL, Farid S. Radiative and Nonradiative Electron-Transfer in Contact Radical-Ion Pairs. Chemical Physics 1993;15:2–3.
33. Flurry, RL, JR. Symmetry Groups Theory and Applications. Prentice Hall; Englewood Cliffs: 1980.
34. Brus LE. Electron Electron and Electron-Hole Interactions in Small Semiconductor Crystallites - the Size Dependence of the Lowest Excited Electronic State. Journal Of Chemical Physics 1984;80:4403–4409.
35. Yu WW, Qu LH, Guo WZ, Peng XG. Experimental determination of the extinction coefficient of CdTe, CdSe, and CdS nanocrystals. Chemistry Of Materials 2003;15:2854–2860.
36. Norris DJ, Efros AL, Rosen M, Bawendi MG. Size dependence of exciton fine structure in CdSe quantum dots. Physical Review B 1996;15:16347–16354.
37. Klimov V, Bolivar PH, Kurz H. Ultrafast carrier dynamics in semiconductor quantum dots. Physical Review B 1996;15:1463–1467.
38. Woggon U, Giessen H, Gindele F, Wind O, Fluegel B, Peyghambarian N. Ultrafast energy relaxation in quantum dots. Physical Review B 1996;15:17681–17690.
39. Chung IH, Bawendi MG. Relationship between single quantum-dot intermittency and fluorescence intensity decays from collections of dots. Physical Review B 2004;70:165304.
40. Chung I, Witkoskie JB, Cao JS, Bawendi MG. Description of the fluorescence intensity time trace of collections of CdSe nanocrystal quantum dots based on single quantum dot fluorescence blinking statistics. Physical Review E 2006;73:011106.
41. Hegarty J, Sturge MD, Weisbuch C, Gossard AC, Wiegmann W. Resonant Rayleigh-Scattering from an Inhomogeneously Broadened Transition - a New Probe of the Homogeneous Linewidth. Physical Review Letters 1982;49:930–932.
42. Schwartz A, Wang A, Early E, Gaigalas AK, Zhang Y, Marti G, Vogt R. Quantitating Fluorescence Intensity from Fluorophore: the definition of MESF Assignment. J. Res. Natl. Inst. Stand. Technol 2002;107:83–91.
43. Wang L, Gaigalas AK, Abbbasi F, Marti G, Vogt R, Schwartz A. Quantitating Fluorescence Intensity From Fluorophores: Practical Use of MESF Values. J. Res. Natl. Inst. Stand. Technol 2002;107:339–353.
44. Bawendi MG, Steigerwald ML, Brus LE. The Quantum-Mechanics of Larger Semiconductor Clusters (Quantum Dots). Annual Review Of Physical Chemistry 1990;41:477–496.
45. Bawendi MG, Carroll PJ, Wilson WL, Brus LE. Luminescence Properties of Cdse Quantum Crystallites - Resonance between Interior and Surface Localized States. Journal Of Chemical Physics 1992;15:946–954.
46. Empedocles SA, Neuhauser R, Shimizu K, Bawendi MG. Photoluminescence from single semiconductor nanostructures. Advanced Materials 1999;20:1243–1256.
47. Klimov VI, Mikhailovsky AA, McBranch DW, Leatherdale CA, Bawendi MG. Quantization of multiparticle Auger rates in semiconductor quantum dots. Science 2000;11:1011–1013. [PubMed: 10669406]
48. Klimov VI, Mikhailovsky AA, McBranch DW, Leatherdale CA, Bawendi MG. Mechanisms for intraband energy relaxation in semiconductor quantum dots: The role of electron-hole interactions. Physical Review B 2000;15:R13349–R13352.
49. Leatherdale CA, Woo WK, Mikulec FV, Bawendi MG. On the absorption cross section of CdSe nanocrystal quantum dots. Journal Of Physical Chemistry B 2002;8:7619–7622.
50. Yu PR, Beard MC, Ellingson RJ, Ferrere S, Curtis C, Drexler J, Luiszer F, Nozik AJ. Absorption cross-section and related optical properties of colloidal InAs quantum dots. Journal Of Physical Chemistry B 2005;21:7084–7087.
51. Micic OI, Cheong HM, Fu H, Zunger A, Sprague JR, Mascarenhas A, Nozik AJ. Size-dependent spectroscopy of InP quantum dots. Journal Of Physical Chemistry B 1997;19:4904–4912.

52. Hoheisel W, Colvin VL, Johnson CS, Alivisatos AP. Threshold for Quasi-Continuum Absorption and Reduced Luminescence Efficiency in Cdse Nanocrystals. Journal Of Chemical Physics 1994;15:8455–8460.

53. Fisher BR, Eisler HJ, Stott NE, Bawendi MG. Emission intensity dependence and single-exponential behavior in single colloidal quantum dot fluorescence lifetimes. Journal Of Physical Chemistry B 2004;8:143–148.

54. Magde D, Rojas GE, Seybold PG. Solvent dependence of the fluorescence lifetimes of xanthene dyes. Photochemistry and Photobiology 1999;70:737–744.

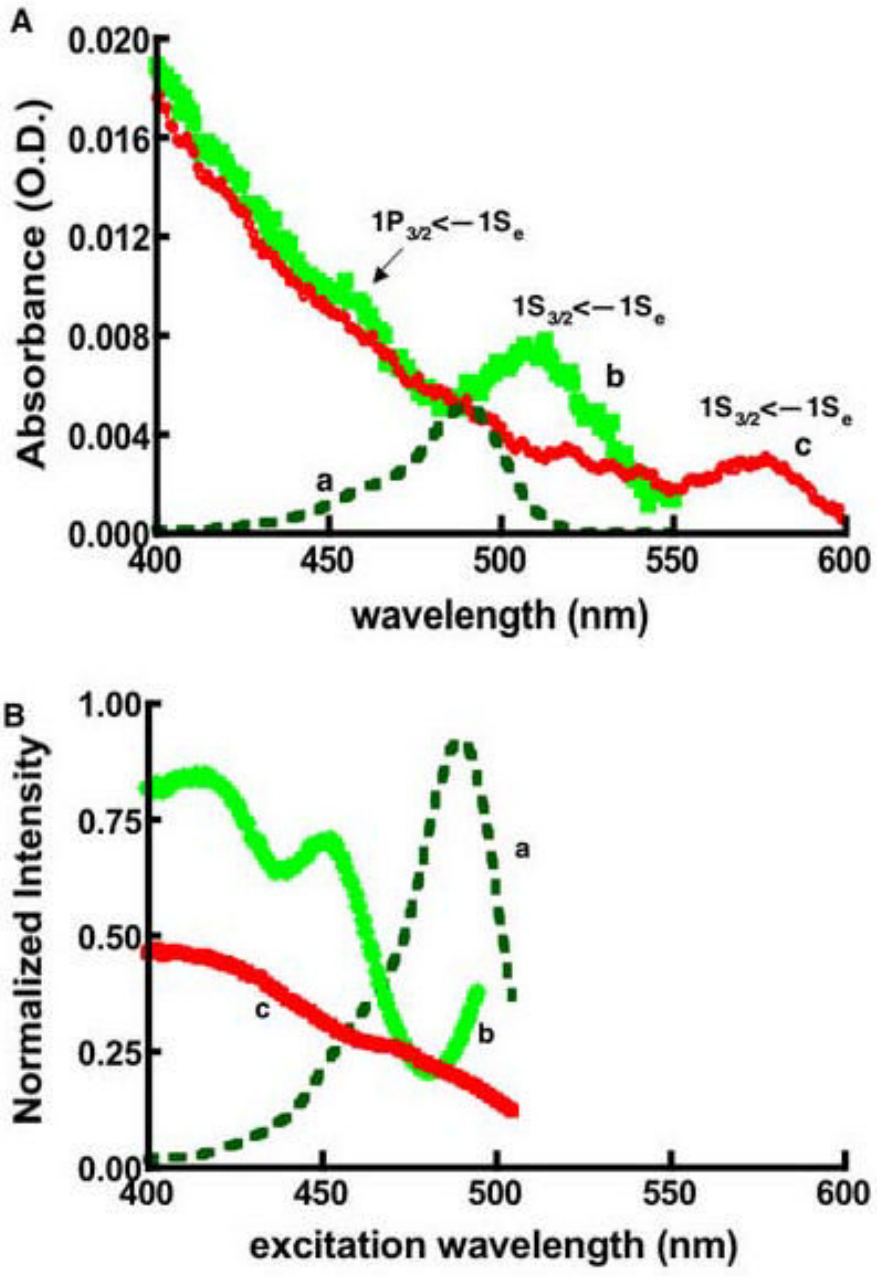

Figure 1.

Comparison of absorbance (**A**), and lamp corrected excitation spectra (**B**) of quantum dots and fluorescein: (a) Fluorescein (b) QD525 (c) QD585. $1S_{3/2}$<—$1S_e$ and $1P_{3/2}$<—$1S_e$ are the spectroscopic term symbol notations associated with the first (band edge) and second excitonic transitions (*n.b.* the $1P_{3/2}$<—$1S_e$ annotation is only showing the location of the transition of QD525). The samples' optical densities were matched at 488 nm by design. The excitation spectra were measured using the same samples characterized in panel **A**. The excitation and emission monochromators' resolution was set at 16nm. The detection wavelengths for fluorescein and QD525 were set at 525nm, while QD585 was set at 585nm. The correction for the lamp's uneven spectral distribution (L_λ) was as described in the text.

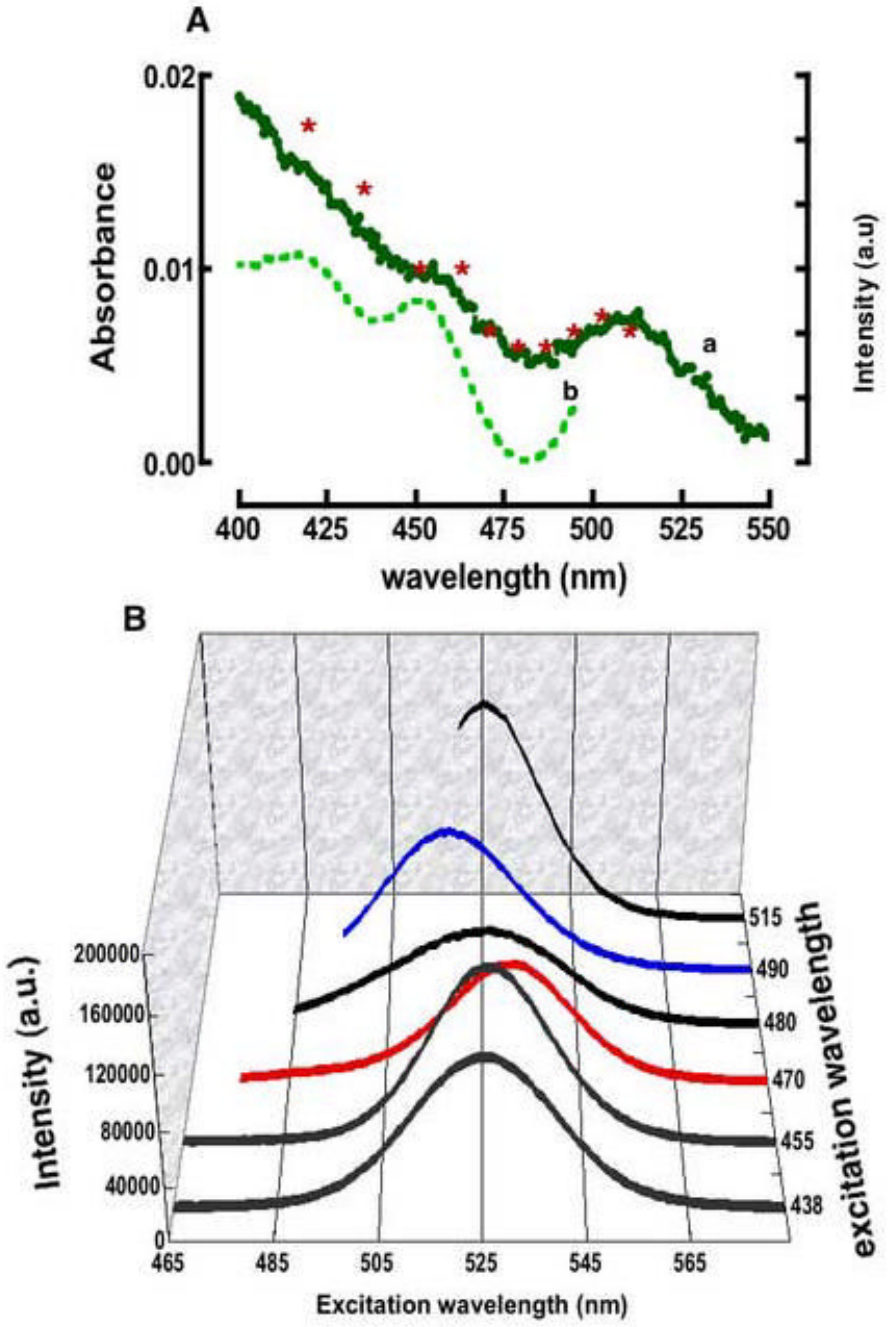

Figure 2.

A. Overlay of the absorption and excitation spectra of QD525 dots (same data from Figure1). Asterisks are drawn on the absorption spectrum to indicate the wavelengths of excitation associated with the emission spectra shown in B. The excitation and emission monochromators' slitwidths were set at 2nm resolution. **B** 3D plot of emission spectra of QD525 from excitation at the wavelengths shown along the z-axis. Spectra were background corrected for light scatter and are normalized for the optical density at the excitation wavelengths, and for excitation lamp's spectral distribution, L_λ. The spectral bandwidths and maxima are anomalously dependent on the excitation wavelength.

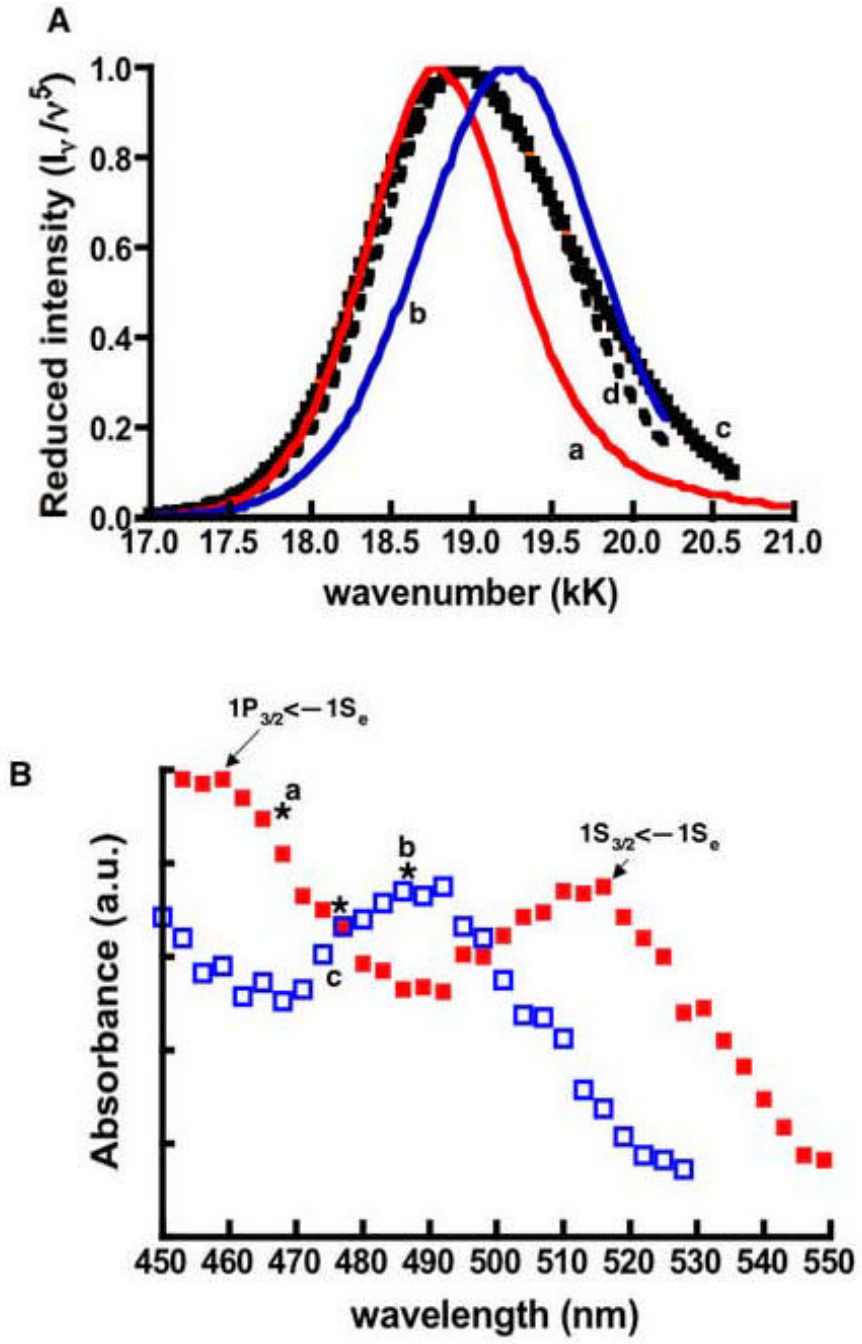

Figure 3.

A. Normalized reduced spectra from excitations at (a) 470EX (b) 490EX (c) 480EX. (d) Mathematical averaged spectrum of 470EX and 490EX spectra. **B**. Generally, the band edge transitions of larger dots are characteristically lower in energy than their smaller counterparts (8). Model absorption spectra of larger-sized (bold squares) and smaller-sized dots (open squares) are shown here to display the spectral mismatch of the absorption bands, which correspond to their respective lowest electronic transitions. Resonance excitation at the wavelengths marked by asterisks yielded the (a) red shifted, (b) blue shifted, and (d) broad spectra shown in panel **A**.

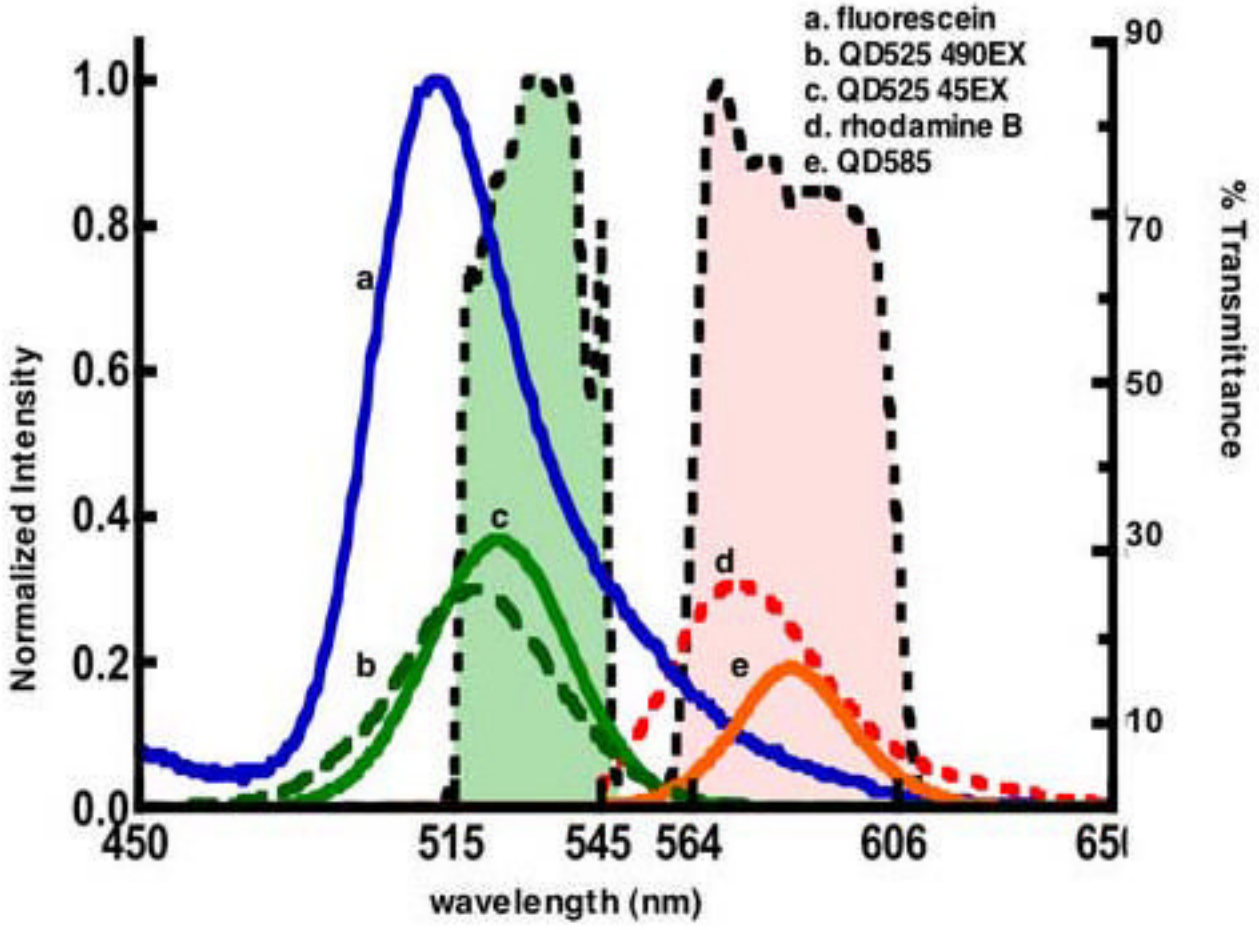

Figure 4.

Emission spectra of fluorescein, rhodamine B and quantum dots. The spectra of rhodamine B (54), QD525 and QD585 are scaled to correspond to their quantum yields relative to fluorescein. Green and orange bars represent band pass filters used in a standard flow cytometer (530/30 BP for FL1, and 585/42 BP for FL2). The resonance overlap between the bandpass filters and emission spectra regulates the amount of light that is transmitted or rejected by the BP filter: Less than 28% fluorescein emission is transmitted through the FL1 filter, compared to 48% of QD525, and 65% of QD585 emission that is transmitted to the FL2 channel.

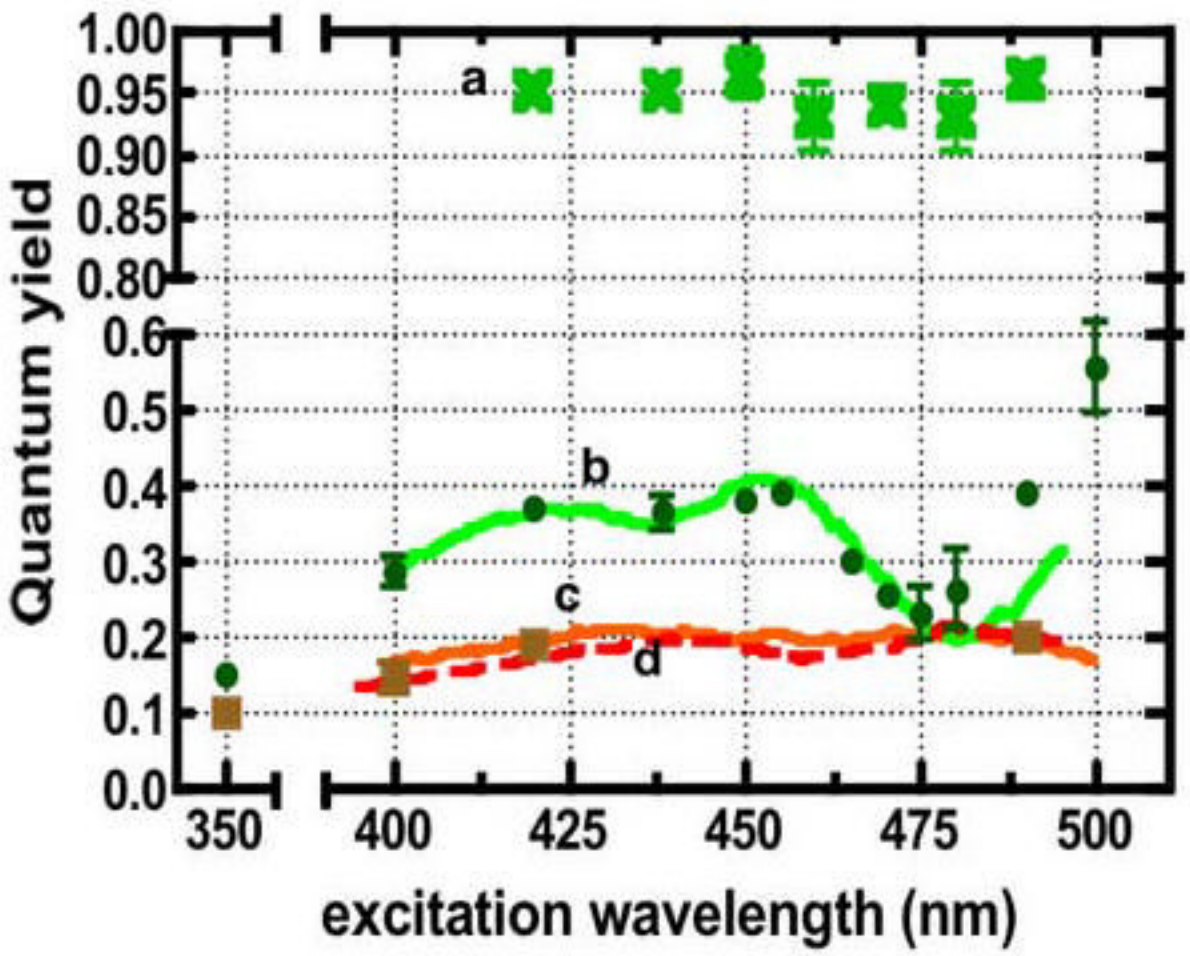

Figure 5.
Plot of quantum yields of (a) fluorescein (b) QD525, (c) QD585, and (d) QD605 versus excitation wavelength. The quantum yields were calculated as described in Table 2. The lines are data derived from excitation spectra while data points represent data derived from integrated intensity.—

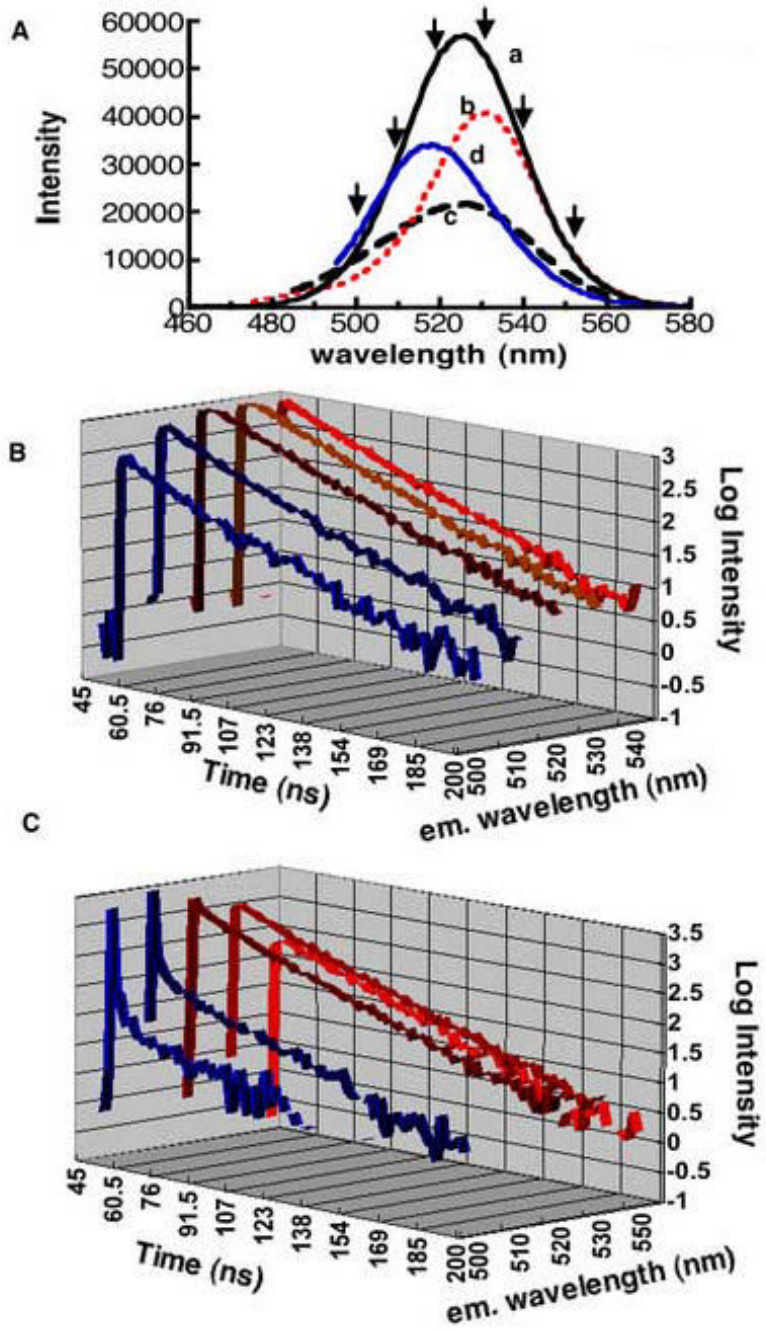

Figure 6.

A. Emission spectra measured at (a) 438 (b) 470, (c) 480, and d 490nm excitations. Arrows indicate wavelengths at which emission lifetimes were probed. **B** 3D Semi-log plot of fluorescence lifetime decay data obtained from exciting QD525 dots at 438nm. Emission decays were measured at the detection wavelengths shown along the z-axis. **C.** 3D Semi-log plot of fluorescence lifetime decay data obtained from exciting QD525 dots at 480nm. Emission decays were measured at the wavelengths shown along the z-axis. The fast component decays shown in C correspond to strong resonance Rayleigh scatter (see text).

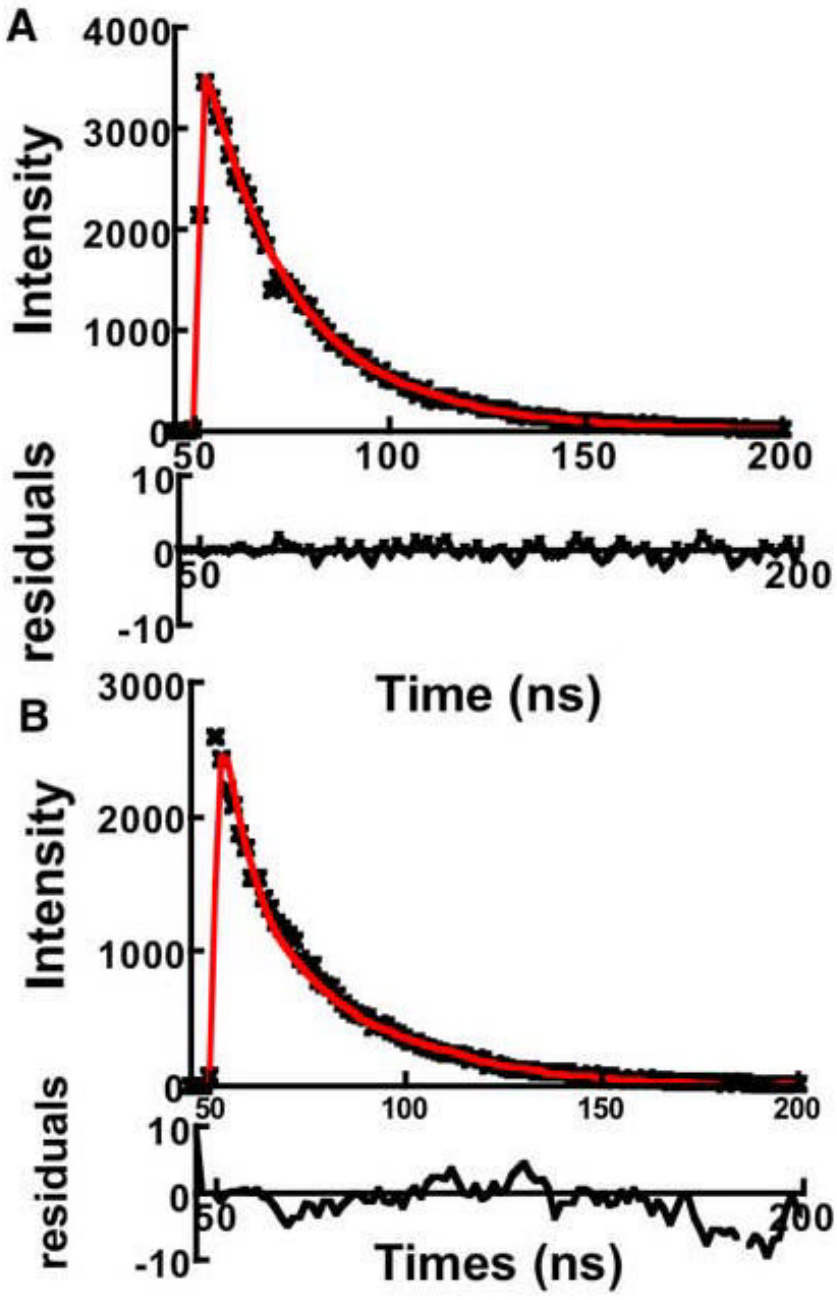

Figure 7.

Plots of fluorescence decay measured at 530 nm. Samples were excited at: **A**. 500 nm and **B** 480 nm. Excitation at 500 nm produces excited state species with single exponential decay emission suggesting a single population of dots, whereas exciting at 480nm probes a wide distribution of dot sizes. Data were fit to a double exponential decay (minor component, $t_{1/2}\approx$ 4ns; and major, $t_{1/2}\approx$ 23 ns). As the residuals show a two-parameter fit was insufficient to analyze the data suggesting the contribution of multiple sizes of dots (see text for details)

Table 1

Dependence of emission band maxima and bandwidths on excitation wavelengths for QD525 and QD585 dots.

Excitation wavelength	Band maxima	Bandwidth (FWHM)	Excitation wavelength	Band maxima	Bandwidth (FWHM)
420	526	31	480	526	44
430	526	34	490	518	33
455	525	29	500	520	29
465	529	29	505	523	28
470	531	31	510	524	30
475	530	36	515	525	30
		QD585			
400	584	28	550	584	31
450	585	28	560	583	28
488	585	28	570	583	30

Table 2

Summary of spectroscopic properties of fluorescein conjugates and QD525, (lot#1005-0045) and QD585, (Lot#0905-0031) Quantum dots.

Fluors.	Bandwidth FWHM (nm)[1]	λ_{ex}(nm); $\varepsilon(M^{-1}cm^{-1})$[2]	φ_s[3] = $\varphi_{ref}\frac{I_s}{I_{ref}}\frac{OD_{ref}}{OD_s}\frac{n_s^2}{n_{ref}^2}$	% Trans. (BP Filter)[4]
$Biotin^{FITC}$ $FLAG^{FITC}$	Asymmetric	488; 80,000[a]	0.82[a] 0.20[a]	28(530/30)[a]
QD525	33	488; 130,000[b] 458;216,000 405;360,000 350;710,000	0.30[a] 0.40[a] 0.27[b] 0.15[b]	38(530/30)[b] 48(530/30)[c]
QD585	28	488; 530,000[c] 458; 1,100,000 405; 2,200,000 350; 3.500,000	0.20[b] , 0.67[c] 0.20[d] 0.14[d] 0.10[d]	65(585/42)
QD605	28	488; 1,100,000[c] 458; 1,700,000 405; 2,800,000	0.20[b] , 0.67[c] 0.18[d] 0.14[d]	

Notes:

[1] The bandwidth for QD525 corresponds to excitation at 420nm.

[2] Extinction coefficients obtained from www.probes.invitrogen.com. (a). The extinction coefficient of fluorescein and some derivatives vary from 85,000 for the NIST fluorescein solution standard reference material SRM 1932 to 75,000 for some FITC derivatives, and values are for pH dependent. We have selected a median number here.

[3] Relative quantum yields (φ_S) were calculated using the integrated intensity of sample relative to: a). Fluorescein, φ_{ref}= 0.95; I_S and I_{ref} are the integrated band intensities. The optical densities (OD) of the sample (s) and reference (ref) were kept close. *n* is the index of refraction of the solvent; 1.32 for water. (b). φ_S determined from photoexcitation spectra and scaling to values obtained in a) (*c.f.* Figure 5). (c). φ_S determined relative to Rhodamine B, φ_{ref}= 0.31 in water (Magde et. al., Photochem. Photobiol. 1999). (d). φ_S determined from photoexcitation spectra and scaling to values obtained in Figure 5.

[4] See Figure 4, the bandpass filters are those on a standard model BD Facscan flow cytometer. (a) Spectral mismatch between fluorescein and derivatives is assumed to be negligible in this table (b) Emission spectra from the excitation of QD525 at 488 nm (c) Excitation of QD525 at 450 nm.